Astron. Astrophys. 345, 448–460 (1999)

ASTRONOMY AND ASTROPHYSICS

ESO imaging survey

III. Multicolor data near the South Galactic Pole

I. Prandoni[1,2], R. Wichmann[1,3], L. da Costa[1], C. Benoist[1,4], R. Méndez[1,5], M. Nonino[1,6], L.F. Olsen[1,7], A. Wicenec[1], S. Zaggia[1,8], E. Bertin[1,9,10], E. Deul[1,9], T. Erben[1,11], M.D. Guarnieri[1,12], I. Hook[1], R. Hook[13], M. Scodeggio[1], and R. Slijkhuis[1,9]

[1] European Southern Observatory, Karl-Schwarzschild-Strasse 2, D-85748 Garching bei München, Germany
[2] Istituto di Radioastronomia del CNR, Via Gobetti 101, I-40129 Bologna, Italy
[3] IUCAA, Post Bag 4, Ganeshkhind, Pune 411007, India
[4] DAEC, Observatoire de Paris-Meudon, 5 Pl. J. Janssen, F-92195 Meudon Cedex, France
[5] Cerro Tololo Inter-American Observatory, Casilla 603, La Serena, Chile
[6] Osservatorio Astronomico di Trieste, Via G.B. Tiepolo 11, I-31144 Trieste, Italy
[7] Astronomisk Observatorium, Juliane Maries Vej 30, DK-2100 Copenhagen, Denmark
[8] Osservatorio Astronomico di Capodimonte, Via Moiariello 15, I-80131 Napoli, Italy
[9] Leiden Observatory, P.O. Box 9513, 2300 RA Leiden, The Netherlands
[10] Institut d'Astrophysique de Paris, 98bis Bd Arago, F-75014 Paris, France
[11] Max-Planck-Institut für Astrophysik, Postfach 1523, D-85748 Garching bei München, Germany
[12] Osservatorio Astronomico di Pino Torinese, Strada Osservatorio 20, I-10025 Torino, Italy
[13] Space Telescope – European Coordinating Facility, Karl-Schwarzschild-Strasse 2, D-85748 Garching bei München, Germany

Received 17 July 1998 / Accepted 16 December 1998

Abstract. This paper presents multicolor data obtained for a 1.7 square degree region near the South Galactic Pole (patch B) as part of the ESO Imaging Survey (EIS). So far the observations have been conducted in B, V and I, but are expected to be complemented by observations in the U-band later in 1998. Object catalogs extracted from single exposure images are 80% complete down to $B \sim 24$, $V \sim 23.5$ and $I \sim 22.5$, and once co-added should reach about 0.5 mag deeper. The data are being made public in the form of catalogs, pixel maps, target lists and image "postage stamps", which can be retrieved from the Web. Counts of stars and galaxies and the angular two-point correlation function of galaxies are computed and compared to other available data to evaluate the depth and uniformity of the extracted object catalogs. In addition, color distributions of stellar objects are presented and compared to model predictions to examine the reliability of the colors. The results suggest that the overall quality of the catalogs extracted from the images is good and suitable for the science goals of the survey.

Key words: catalogs – surveys – stars: statistics – galaxies: statistics

1. Introduction

The present paper is part of a series presenting the data accumulated by the public ESO Imaging Survey (EIS) being carried out in preparation for the first year of regular operation of the VLT.

Send offprint requests to: L. da Costa

As described in previous papers (Renzini & da Costa 1997, Nonino et al. 1999, hereafter paper I) the main science goal of EIS is the search for rare objects such as clusters of galaxies, spanning a broad redshift range, quasars at intermediate and high redshifts, high-redshift galaxies and stars with special characteristics (e.g., white dwarfs, very low mass stars, brown dwarfs). These goals have guided the adopted survey strategy which, for EIS-wide, envisioned observations in V and I to search for clusters and in four passbands (U, B, V, I) over ~ 1.7 square degrees in a region near the South Galactic Pole (EIS-wide patch B). The observations in B, V and I have already been completed, while observations in the U-band are expected to be carried out in the fall of 1999.

One of the main motivations for the multicolor survey has been the identification of a large number of close line-of-sight, intermediate redshift QSOs to study the three-dimensional distribution of absorbers, using medium and high-resolution spectrographs (e.g., UVES) at the VLT. For this reason, a region near the SGP, where several QSOs are known from previous studies, has been selected. However, the data are also useful for galactic studies and for the identification of rare stellar populations, with the survey having a unique combination of depth and area coverage. The additional V-band images, which altogether overlap the I images over $\sim 70\%$ of the surveyed area in patches A and B (15% of the whole EIS-wide), are also useful in the search of galaxy clusters (e.g., Olsen et al. 1999, paper V). Finally, it is important to emphasize that the present data offer an excellent opportunity to assess the complexity of efficiently handling large volumes of multicolor data and extracting useful

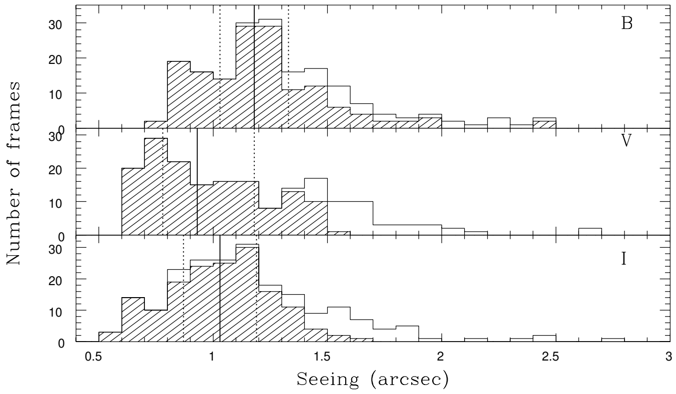

Fig. 1. Histogram of the seeing distribution for patch B obtained from all observed frames and from the frames actually accepted for the survey (shaded area). Vertical lines refer to 25, 50 and 75 percentiles of the accepted frames distribution. The three panels refer to the three observed bands (B, V, I), as indicated in each panel.

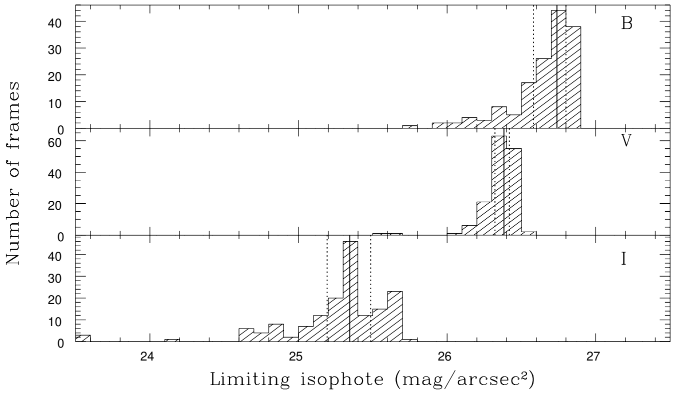

Fig. 2. Limiting isophote distributions from patch B frames actually accepted for the survey. Vertical lines refer to 25, 50 and 75 percentiles of the distributions. The three panels refer to the three observed bands (B, V, I).

target lists. This is a key element for the exploration of the full range of science offered by the multicolor surveys envisioned for the new wide-field camera (WFI@2.2m) at the ESO/MPIA 2.2m telescope at La Silla.

In Sect. 2, the observations are described and the characteristics of the multicolor data are presented. This section also presents the extracted object catalogs and discusses their completeness and reliability. In Sect. 3 the catalogs are evaluated by comparison with models and other data. Concluding remarks are presented in Sect. 4.

2. Observations and data reduction

2.1. Observations

The observations of patch B were carried out over several months in the period July 1997 to December 1997, using the red channel of the EMMI camera on the 3.5m New Technology Telescope (NTT) at La Silla. The red channel of EMMI is equipped with a Tektronix 2046 $\times$ 2046 chip with a pixel size of 0.266 arcsec and a useful field-of-view of about $9' \times 8.5'$. EIS uses a special set of BVI filters and the response function of the system can be found in paper I.

As described in paper I, the observations were carried out by a sequence of overlapping exposures (hereafter referred to as even/odd frames) 150 sec each, with each position on the sky being sampled at least twice. A total of 701 frames were obtained in the area with 200 in B, 282 in V and 219 in I bands. Only 150 frames in each band were required to cover the field but poor weather conditions required several frames to be re-observed. The strong variations in the observing conditions can be seen in Fig. 1 which shows, for each band, the seeing distribution of all observed frames. For comparison the shaded histograms show the seeing distribution of the frames finally accepted, with the solid vertical line in each panel indicating the median seeing for each band. The B-band is the worst overall with a median seeing of 1.2 arcsec and with a few frames extending to very large seeing (~ 2.5 arcsec). The upper and lower quartiles are, as can be seen in Fig. 1 $\sim$1.0 and $\sim$1.3 in B, ~ 0.8 and $\sim$1.2 for V and $\sim$0.9 and $\sim$1.2 in I. In the analysis below 9 frames with seeing $\gtrsim$1.8 arcsec were discarded because of their incompleteness at faint magnitudes. Fig. 2 shows, again for each band, the 1σ limiting isophote within 1 arcsec. The transparency of the nights also showed significant variations especially for the I-band images, with one frame reaching 21 mag/arcsec^2 (not shown in the figure). For this frame, which was removed from the analysis, the depth reached is considerably shallower than the remaining frames leading not only to a bright limiting magnitude but also to the detection of a significant number of spurious objects. Other frames with bright limiting isophotes have no significant impact in the analysis presented in Sect. 3.

Figs. 3 and 4 show, for each band, the two-dimensional distribution of the seeing and limiting isophote as determined from the even frames. Similar results are obtained for the odd frames which alternate with the even ones. Such maps allow the potential user of the derived catalogs to evaluate their reliability. The final data are reasonably homogeneous with the median seeing in all bands < 1.2 arcsec. However, some poor images do exist and for some applications must be removed, as discussed above. The area that is affected is $\lesssim$0.1 square degree.

Finally, it is worth mentioning that since the completion of paper I, the V images for patch A over an area $\sim$ 1.1 square degrees have also been reduced and are being made available together with the catalogs extracted from them which are used below.

2.2. Data reduction

The data were processed by the EIS pipeline being developed to handle large imaging programs and described in detail in paper I. The software development is still in progress with new functionalities being constantly added to the pipeline as well as enhanced features in Skycat driven by the survey needs, in particular to facilitate the visual inspection of the target lists being produced. In addition, new tools are being developed to handle color information, which adds a new level of complexity

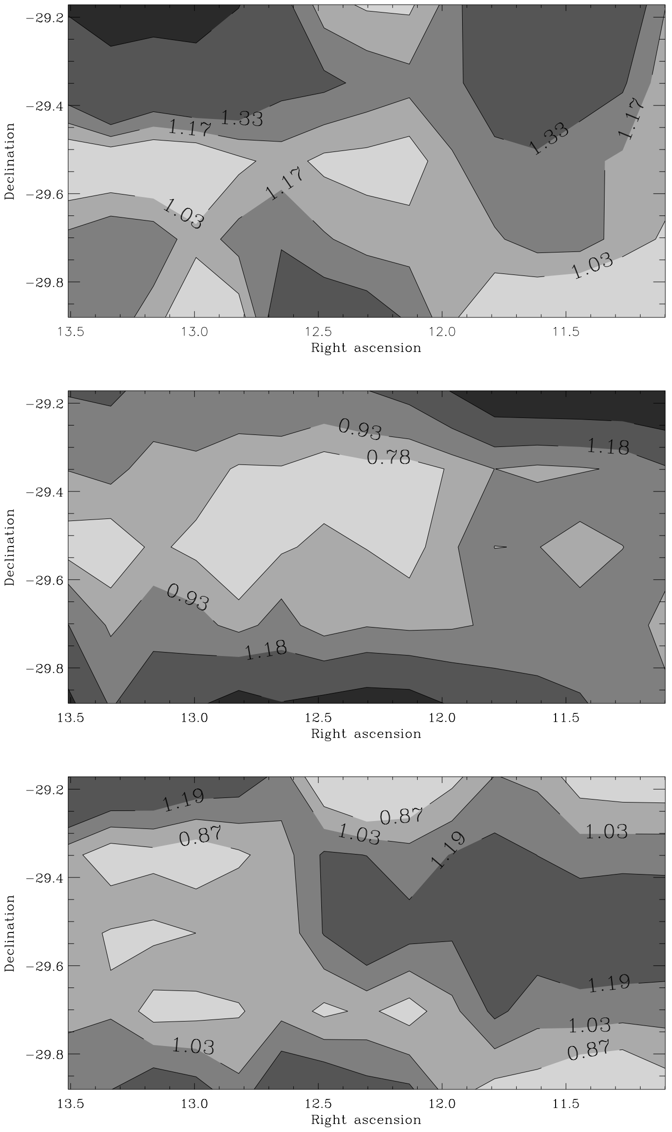

Fig. 3. Two-dimensional distribution of the seeing as measured for patch B for all the accepted even frames. Contours refer to 25, 50 and 75 percentiles of the distribution. The three panels refer to the three observed bands (B, V, I) from top to bottom.

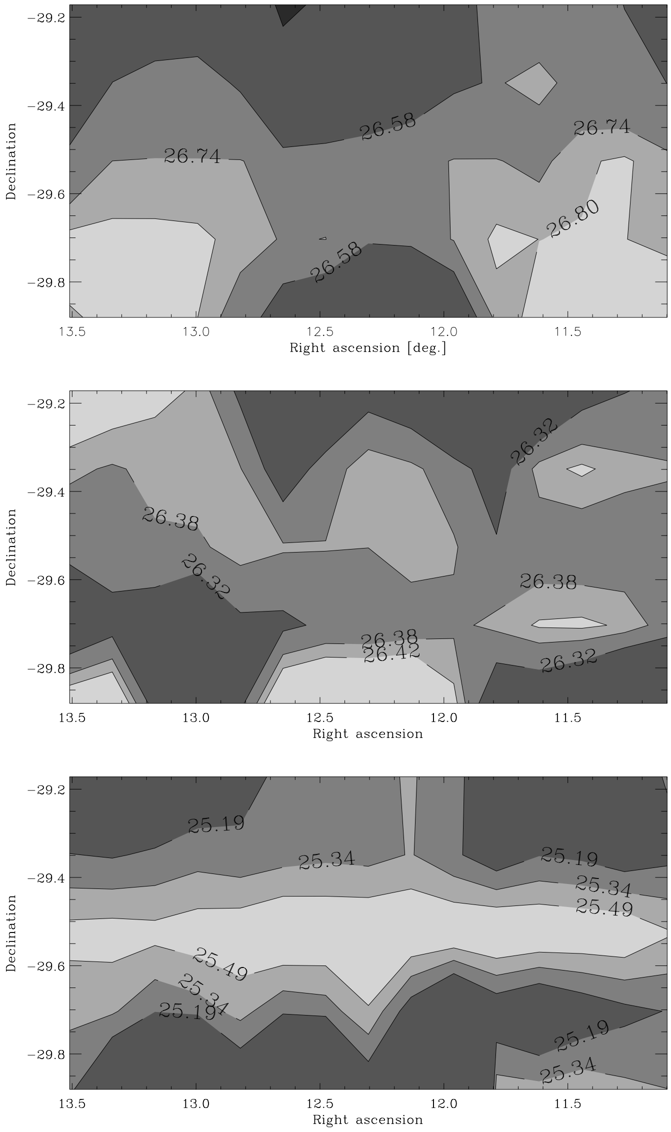

Fig. 4. Two-dimensional distribution of the limiting isophote as defined in the text estimated from the accepted even frames for patch B. Contours refer to 25, 50 and 75 percentiles of the distribution. The three panels refer to the three observed bands (B, V, I), from top to bottom.

especially in the preparation of object catalogs. Computation of colors require reliable association of objects detected in different passbands, which may be affected differently by the seeing, astrometric errors, the morphology of the objects and the performance of the de-blending algorithm. One also needs a proper definition for the measurement of colors for faint sources and upper limits for non-detections. Currently, preliminary color catalogs are being produced only for point-sources, which are being systematically inspected to verify the catalogs and identify any peculiarities (Zaggia et al. 1999). This is an important first step towards the preparation of the final color catalog for patch B. For instance, during the visual inspection of objects selected by their peculiar colors, it became evident that ghost images, observed near relatively bright stars ($V \lesssim 14$) in the B and V images, contaminate the catalogs.

2.3. Color transformation

Using all the standard star observations carried out in photometric nights at the NTT with the EIS filters, in the period July 1997-March 1998, the color transformation between the EIS and the Johnson-Cousins systems has been determined. In Fig. 5 the observed transformations for all the three bands are shown, as a function of color in the Johnson-Cousins system. The fits are given by the relations:

$$B_{EIS} = B - 0.132(B - V) \quad (1)$$
$$V_{EIS} = V + 0.047(B - V) \quad (2)$$
$$V_{EIS} = V + 0.045(V - I) \quad (3)$$
$$I_{EIS} = I + 0.036(V - I) \quad (4)$$

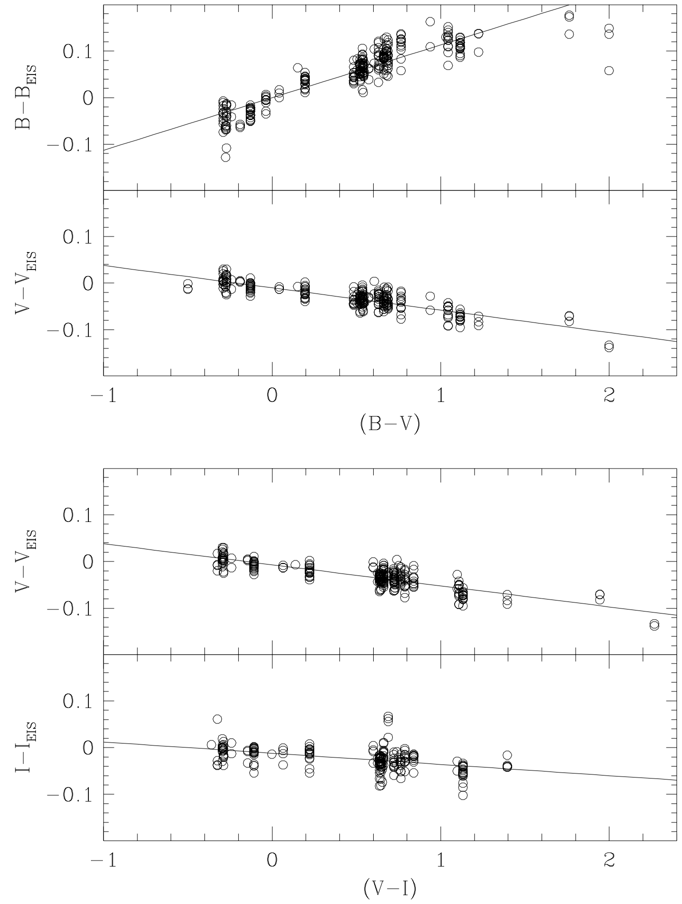

Fig. 5. Relation between the EIS and Johnson-Cousins system as a function of color. Shown are all the standard stars observed under photometric conditions in the period July 1997-March 1998.

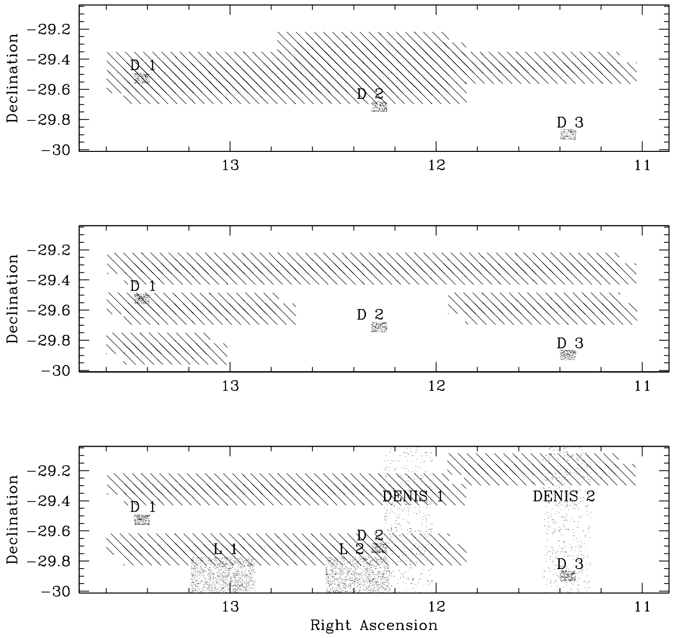

Fig. 6. Distribution of frames obtained at the 0.9m Dutch (D) telescopes at La Silla overlapping the surveyed region of patch B. Also shown are parts of two DENIS strips that cross the field and the Lidman & Peterson fields (L) within the surveyed area. The hatched area represents regions containing EIS frames observed under photometric conditions.

Note that the transformation given here for I_{EIS} is slightly different from that determined in paper I. This is because more standards have been included since and a more careful pruning of the data has been performed. The determination of color corrections include 284 measurements in B, 255 in V and 209 in I, with the formal errors in the color terms estimated to be $\lesssim$ 0.02 mag in all three bands. In general, the color term is small except for the B-band. In this case the data also suggests a possible departure from linearity at the red end. As a final note, it is worth mentioning that in the process of examining all the standard star observations, errors in positions and the presence of variable stars in the Landolt lists were found. A complete list of these problems will be reported elsewhere.

2.4. Calibration

The photometric calibration of the patch was carried out by first bringing all frames to a common zero-point as determined from the relative magnitudes of objects in overlap regions, within a pre-selected magnitude range. This was done by a global least-square fit to all the relative zero-points, constraining their sum to be equal to zero. The internal accuracy of the derived photometric solution is $\lesssim 0.005$ mag (Paper I). Second, absolute zero-points are found for frames observed in photometric conditions. The zero-points for these frames were determined using a total of 36 frames of 7 fields containing standard stars taken from Landolt (1992 a,b), observed over 5 nights. These frames were also reduced through the pipeline, which identified the standard stars and measured magnitudes through Landolt apertures automatically (see paper I). Altogether 148 independent measurements of standards were used in the calibration.

Two solutions are then determined: one which computes a single zero-point offset, based on the weighted average of the zero-points of the calibrated frames, and the other using a first-order polynomial in both right ascension and declination. Comparison with external data suggests that a zero-point offset provides an adequate photometric calibration for the entire patch (see below).

External photometric data come from the Dutch 0.9m telescope at La Silla and from overlaps with DENIS data and with frames taken by Lidman & Peterson (1996). The regions of overlap of these data are shown in Fig. 6. In the figure the regions observed under photometric conditions are also indicated. Comparison of this figure with its counterpart in paper I, demonstrates that the data for patch B is clearly of superior quality with a much larger fraction of frames taken under photometric conditions. Comparison with these external data is important in order to look for possible gradients in the photometric zero-point, introduced by the relative photometry which implicitly assumes that there are no systematic errors in the flatfield from frame to frame.

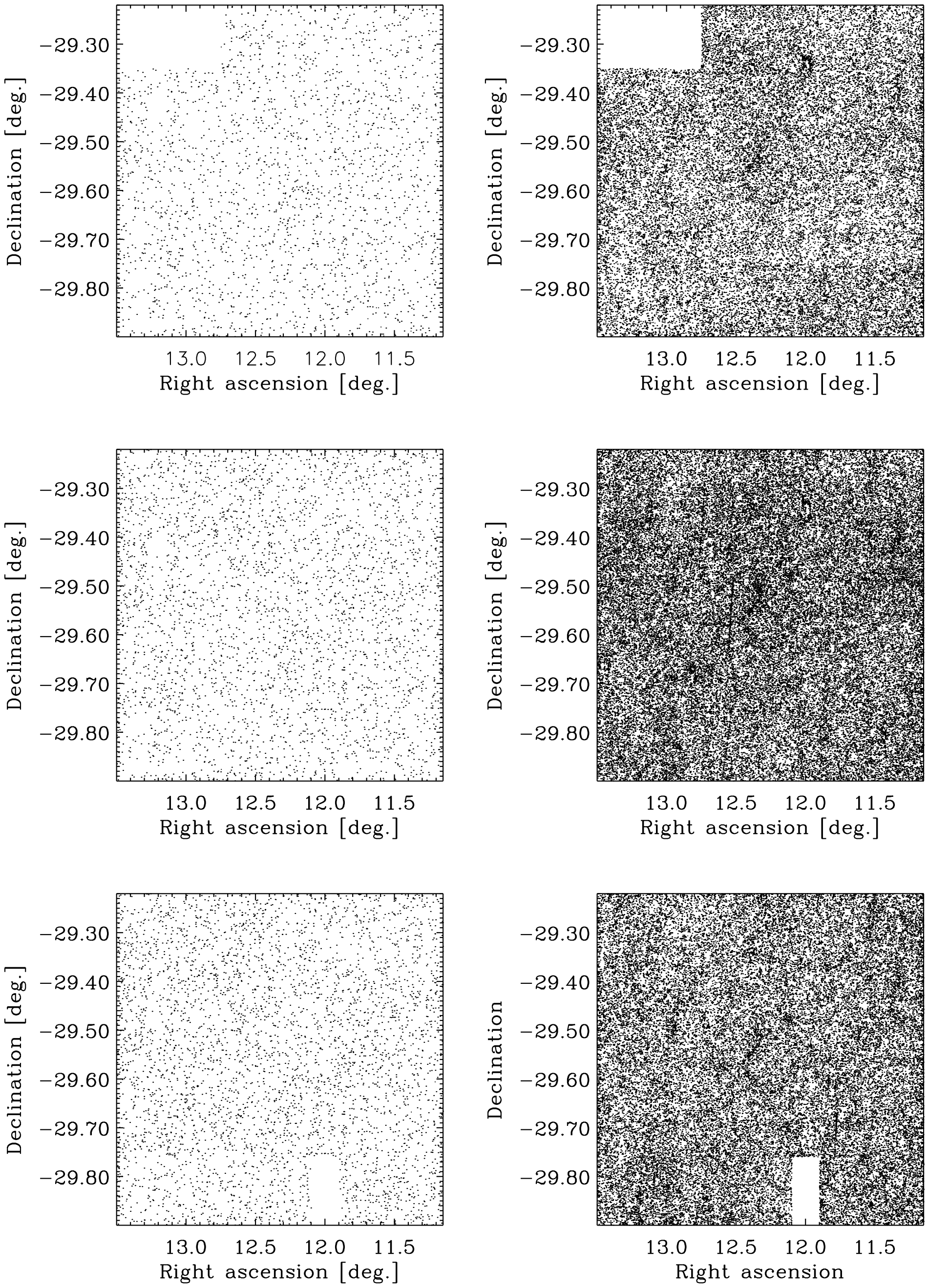

Fig. 7. Projected distribution of stars (*left panel*) and galaxies (*right panel*) detected in the passbands B (*top panels*), V (*middle panels*) and I (*bottom panels*). The limiting magnitude corresponds to the star/galaxy classification limit for stars and to the estimated 80% completeness limit for galaxies (see text). Frames taken under extremely large seeing or with large extinction have been eliminated.

2.5. *Object catalogs*

During the processing of a patch through the pipeline, object catalogs extracted from single frames are merged together into a "patch" catalog for each passband. This is the parent catalog which consists of multiple entries of objects detected in overlapping frames. For each detection, the seeing and noise of the frame in which the object was found are also stored. The parent catalog is used to derive different types of single-entry catalogs detected from 150 sec exposures such as the odd/even catalogs described in paper I. Alternatively, it has also been used to derive a unique catalog (hereafter "best" catalog) defined by examining the characteristics of the frames where a given object was detected, saving only the entry associated with the best seeing frame. Details regarding the methodology of association will be described elsewhere (Deul et al. 1999). From the flag information available in the single-entry catalog, *filtered* catalogs have been produced for analysis purposes. The filtering is required in order to eliminate truncated objects and objects with a significant number of pixels affected by cosmics and/or other artifacts. The parameters adopted in the filtering are the same as those given in paper I.

In general, this single-entry patch-wide catalog is the one used below, while the odd/even are used to estimate the magnitude errors directly from the data, by cross-identifying the objects. For point-like sources, a preliminary attempt has also been made to produce a color catalog combining the information of the catalogs derived from each passband. Using the same association scheme mentioned above, a cross-identification of objects is made and colors are computed using the mag_auto estimator of SExtractor (e.g., Paper I) which should be adequate for point sources. For non-detections in a given band, 1σ limiting magnitudes are computed from the seeing and noise properties of the best seeing frame available at the expected position of the object. Even though still rudimentary, this derived catalog serves for verification purposes and for a first cut analysis of the data. The final color catalog will only be derived from the co-added images. In this case, colors will be computed using the detection area determined from a reference image (one band, e.g., I, or the summed images of different bands,e.g., $V + I$), but measuring the flux in the respective images. Even though the required software is available it is only now being integrated into the pipeline.

It is important to emphasize the complexity of handling and merging information extracted from different passbands. For instance, each object may have a different SExtractor stellarity-index which may impact the galaxy/star classification, close pairs may be de-blended in one passband and not in another, depending on the seeing. Clearly a complete description of all the possible pitfalls and the overall performance of the software is beyond the scope of the present paper, and will instead be discussed in Deul et al. (1999). The current work also shows the shortcomings of handling catalogs and points out the need for the implementation of an object database with a flexible user interface to allow for the full exploration of the data by different groups.

For the purposes of the present paper galaxies are objects with stellarity index < 0.75 if brighter than the star/galaxy classification limit (B=22, V=22, I=21) or any object, regardless of the stellarity index, fainter than this limit. Stars are objects with stellarity index $\geq\ 0.75$. Note that this definition leads to some cross-contamination but it has no significant impact on the conclusions. In evaluating the data in Sect. 3 the derived star and galaxy catalogs were, for simplicity, trimmed at the edges and the bad frames discussed above were removed. After trimming the covered areas are: 1.3, 1.4 and 1.37 square degrees in B, V, I, respectively. The corresponding two-dimensional distributions of stars, down to the star/galaxy classification limits, and galaxies, down to estimated 80% completeness limits (discussed below), are shown in Fig. 7. The total number of objects in these plots are: 2290 stars brighter than $B = 22$ and 33133 galaxies brighter than $B = 24$; 3378 stars brighter than $V = 22$ and 58590 galaxies brighter than $V = 24$; and 4297 stars and 44546 galaxies brighter than $I = 21$ and $I = 22.5$, respectively. Recall that the distribution shown is for the "best" catalog. If one wishes to work with the odd/even catalogs their distribution have to be examined in the same way. In order to avoid extraneous colors due to bad data in one or more bands, the color catalog examined in Sect. 3 corresponds to the common areas covered in the different passbands and has a total area of 1.27 square degrees.

2.6. Completeness, contamination and magnitude Errors

As in paper I, the completeness of the derived catalogs has been established by using a single field where several exposures have been made over the period of observations of patch B. The corresponding catalogs in each passband were then compared with that of a typical frame with an exposure time of 150 sec. A total of 9 exposures in B band, 6 exposures in V band and 8 in I band, were selected discarding others taken in less favorable conditions. These exposures were coadded and the derived catalogs are at least one magnitude deeper than the typical survey frame. Comparing the identified objects in a single exposure frame with those extracted from the co-added images one can derive the expected completeness for typical 150 sec survey frames. The results of these comparisons are shown in Fig. 8 showing that the catalogs are 80% complete at $B \sim 24$, $V \sim 23.5$ and $I \sim 22.5$. These limits should apply for survey frames with a seeing close to the median seeing. Also shown in the figure is the number of false positives computed from the fraction of objects identified in the single exposure frames which were not detected in the co-added image.

In order to estimate the accuracy of the magnitudes the odd and even catalogs were compared and a lower limit estimate of the photometric errors was obtained from the repeatability of the magnitudes for paired objects. The estimated errors from this comparison are given in Fig. 9, which shows that in the interval $16 < I < 20.5$ they range from 0.02 to 0.1 mag, reaching 0.3 mag at $I \sim 23$. Similar values are found for B and V brighter than ~ 24. These values correspond well to those estimated by SExtractor.

It is also of interest to obtain a completely independent estimate of the errors in the magnitudes. This can be done by comparing the objects detected by EIS with those found by Lidman & Peterson (1996), who have used a different object detection algorithm. This is shown in Fig. 10 where the objects detected in two separate fields (see Fig. 6), with 1354 and 1299 objects each, are compared. Note that because of differences in the astrometry this comparison was done using the astrometric solution found by the EIS pipeline but the magnitudes as determined in the original catalog. Even adopting this procedure misidentifications are still present, leading to outliers, over the entire magnitude range, with significant magnitude differences. Nevertheless, the zero-point offset is typically ~ 0.05 mag for $I < 21$, consistent with the zero-point correction proposed by these authors to bring their measurements into the Johnson-Cousins system. Beyond this limit, the Lidman & Peterson catalog becomes increasingly incomplete leading to a biased offset. The scatter in this comparison is less than 0.3 mag down to $I \lesssim 22$, consistent with our internal estimates if one attributes comparable errors to the Lidman & Peterson measurements. The zero-point offset and the scatter of the magnitude differences is the same for the two fields considered, suggesting that there are no strong gradients (in right ascension) in the photometric zero-point of the patch, at least on a 0.5 degree scale, corresponding to the separation of the two Lidman & Peterson fields.

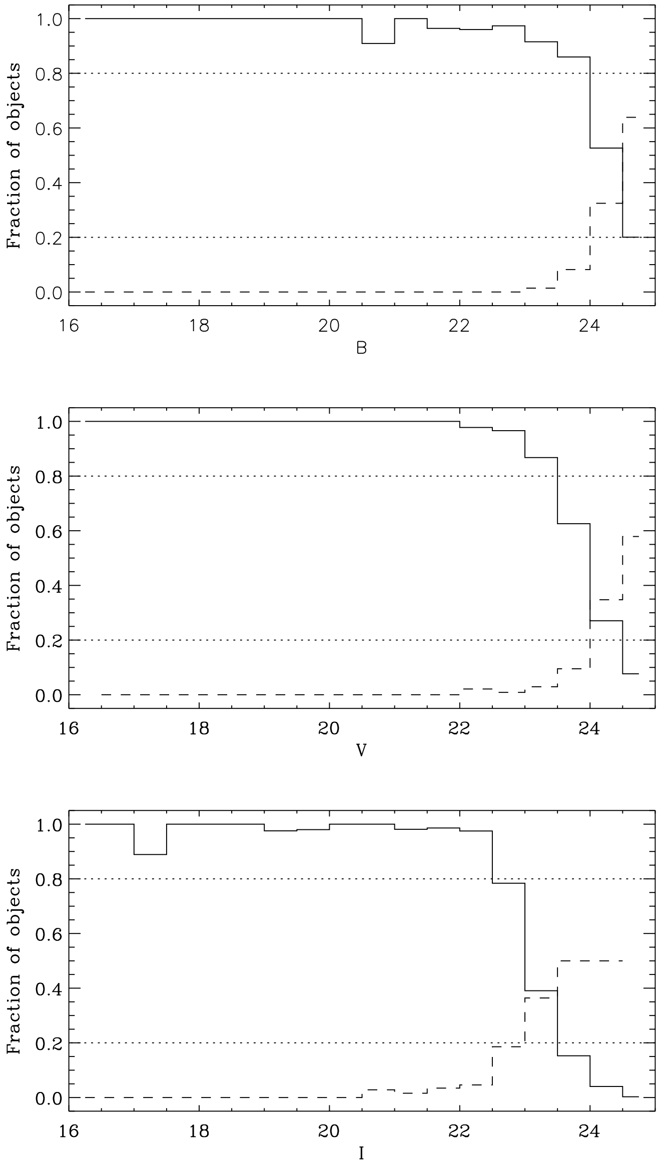

Fig. 8. Completeness (solid line) and expected contamination by spurious objects (dashed line) in the EIS catalogs for the different passbands considered. The computation of these quantities are described in the text.

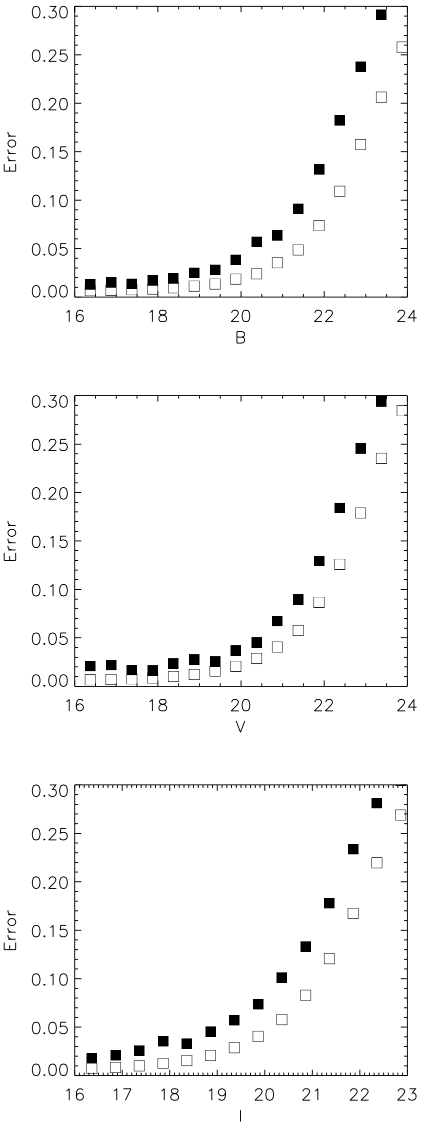

Fig. 9. Comparison between the estimated error in the magnitudes from the odd/even comparison (solid squares) and the SExtractor estimates (open squares).

In order to further investigate possible systematic errors in the photometric zero-point over the scale of the patch, the EIS catalogs were also compared with object catalogs extracted from the two DENIS strips that cross the survey region (see Fig. 6). This allows one to investigate the variation of the zero-point as a function of right ascension and, especially, of declination. The results are shown in Fig. 11. The domain in which the comparison can be made is relatively small because of saturation of objects in EIS at the bright end ($I \sim 16$) and the shallow magnitude limit of DENIS ($I \sim 18$). Still, within the two magnitudes where comparison is possible one finds a roughly constant zero-point offset of less than 0.02 mag for both strips and a scatter that can be attributed to the errors in the DENIS magnitudes (Deul 1998).

Finally, similar comparisons can be made between the EIS magnitudes and those measured from the images obtained at the 0.9m Dutch telescope at La Silla, in this case, for all three passbands. Fig. 12 shows these comparisons, combining all the three fields that overlap patch B. Even though the total number of objects is relatively small (112 in B, 180 in V and 204 in I) preventing an accurate comparison, one finds a reasonable agreement in the zero-point and a scatter that can be accounted for by magnitude errors in the Dutch data (~ 0.2 at $B = 21.5$, $V = 21.5$ and $I = 20$). The observed zero-point offset between the Dutch and EIS data (~ 0.04 in B, $\lesssim 0.1$ in V, $\lesssim$0.02 in I) can be explained by the color term corrections required for the EIS and Dutch measurements to bring both measurements into the Cousins system. As the fields are well separated in right ascension, this result gives further evidence that there are no

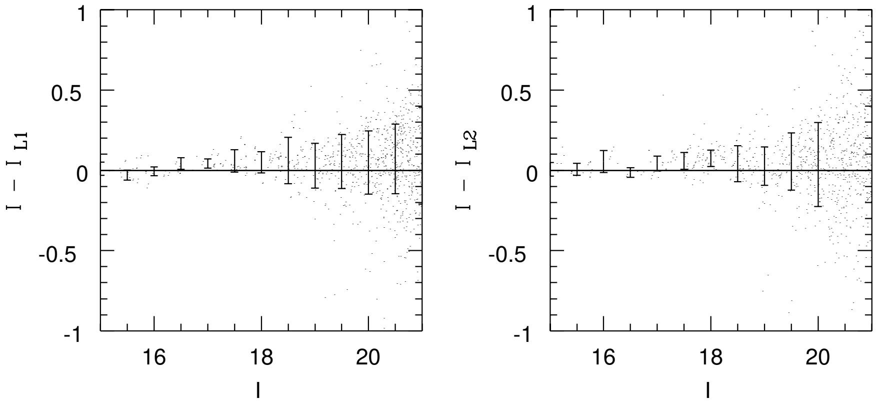

Fig. 10. Comparison of the EIS data in I-band with Lidman & Peterson (1996) catalog for the two fields in common. Also shown are the mean and the rms in 0.5 mag bins.

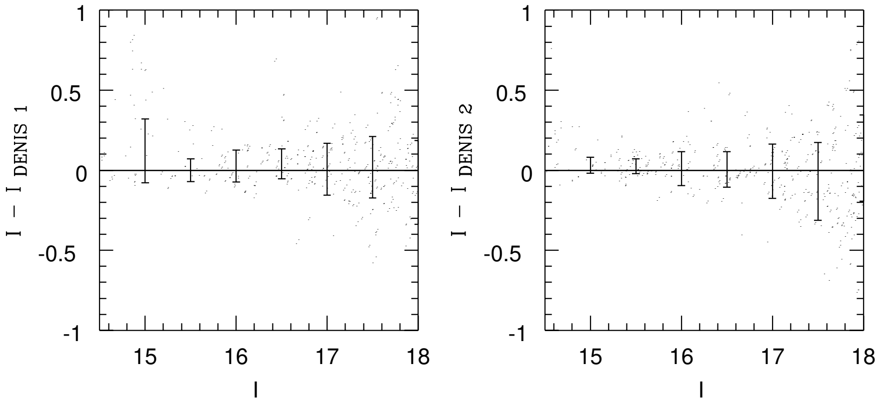

Fig. 11. Comparison of the EIS I-band magnitudes with those measured by DENIS for the two strips that overlap patch B. Also shown are the mean and the rms in 0.5 mag bins.

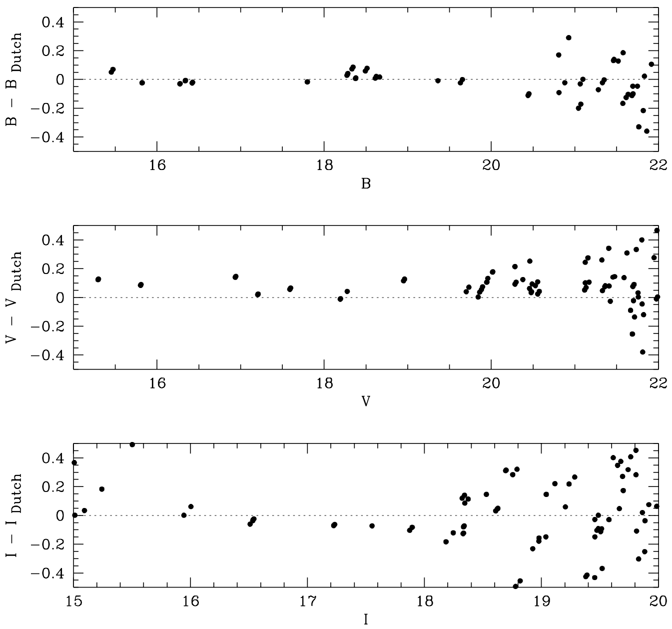

Fig. 12. Comparison of the EIS magnitudes in B, V and I (top to bottom) with those measured from observations of the Dutch 0.9m telescope. Objects in the three fields available have been combined.

significant gradients in the photometric zero-point in any of the passbands.

In summary, comparison of the EIS magnitudes with available external data shows no indication of gradients in the photometric zero-point of the patch. However, the external data are mainly overlapping the EIS data at low declination ($\delta \lesssim -29.5$), especially for the $B-$ and $V-$band, giving weaker constraints in that direction for these bands. Instead, the consistency of the zeropoints for these bands were investigated using the $(V-I)$ for halo stars in the turn-off region around $(V-I) \simeq 0.7$. It was found that the $(V-I)$ of these stars showed a gradient with declination. To localize the problem the $(B-V)$ and $(B-I)$ were also checked for gradients in the direction of declination and the former was found to have gradient. Therefore, a linear relation (Eq. 5) was fitted to remove this gradient.

$$V_{corr} = V_{old} + 0.24 * (30 + dec) \quad (5)$$

This correction has been applied to the catalogs and a second version of the data will be released in 1999, to take this correction into account.

3. Data evaluation

Although this paper does not intend to interpret the data, some basic statistics are computed to evaluate the overall performance of the EIS pipeline in translating images into useful scientific products. For this purpose, the stellar and galaxy samples extracted in each passband and the preliminary color catalog for point-sources are compared below with other available data and model predictions.

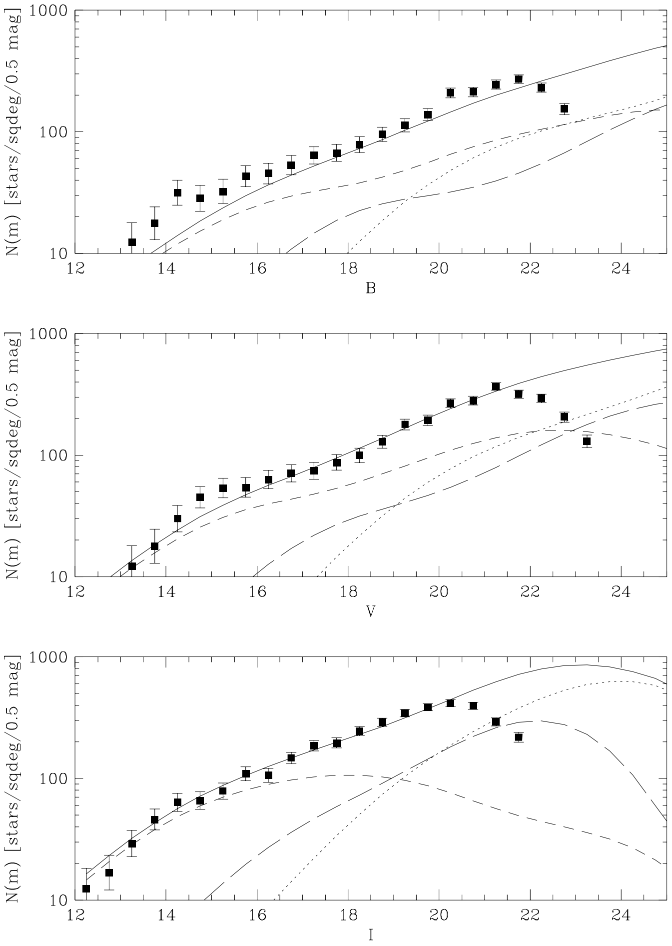

Fig. 13. The EIS differential star counts versus magnitude compared to the galactic model predictions (solid line), as described in the text. The model includes an old disk population (dashed line), a thick disk component (long-dashed line) and a halo (dotted line).

3.1. Point-like sources

Fig. 13, shows the comparison of the star counts for patch B derived using the stellar sample extracted from the object catalogs produced in each passband (Sect. 2.5), with the predicted counts based on a galactic model composed of an old-disk, a thick disk and a halo. The star- and color-counts presented in this section have been computed using the model described by Méndez & van Altena (1996), using the standard parameters described in their Table 1. It is important to emphasize that no attempt has been made to fit any of the model parameters to the observed counts. The model is used solely as a guide to evaluate the data and, as can be seen from Fig. 13 one finds a remarkable agreement with the predicted counts down to the magnitude where the star-galaxy separation is expected to become unreliable. The excess in counts seen at the bright end is due to the saturation of brighter objects ($V \lesssim 16$).

Using the preliminary color catalog for point sources the observed color distribution of stars brighter than $V = 21$ is compared to model predictions in Fig. 14 over three ranges of magnitude as indicated in each panel. The model computes star-counts in B, V and I by adopting a series of color-magnitude diagrams appropriate for the disk, thick-disk and halo of our Galaxy. In order to output predicted counts in the natural passbands of the EIS survey, the transformation given by Eqs. (1)-(4) have been used to convert from the EIS magnitudes to the Johnson-Cousins system in such a way that the predicted counts are actually evaluated in the EIS passbands and are convolved using the error model given in Fig. 9. As can be seen from Fig. 5, the number of red ($(B-V) > 1.2$) standard stars defining the color transformation is very small, so that one might expect possible discrepancies between the observed and predicted counts, particularly for redder colors. One way of overcoming this would be to use synthetic star colors using the system response functions given in paper I. However, for the purposes of describing the usefulness of the data, the current calibration is sufficient. Considering that none of the model parameters have been adjusted to fit the present data, the good agreement of the model to the observed counts in both $(B-V)$ and $(V-I)$ is remarkable, although some discrepancies can also be readily seen.

At the brightest magnitude bin one sees a deficit of red objects relative to the model predictions in both $(B-V)$ and $(V-I)$, especially in the former, which is due to saturation effects. Note that objects with saturated pixels have been discarded from the color catalog.

In the range $18 < V < 20$, the color-counts are known to split into two major peaks, each sampling a different stellar population (Bahcall 1986). The blue peak at $(B-V) \sim 0.5$ is due to halo stars near the turnoff ($M_V \sim +4$), located at few kpc from the Galactic plane. The red peak at $(B-V) \sim 1.3$ is due to faint M-dwarf stars from the disk, located at less than 1 kpc from the Sun. Note the small relative offset (~ 0.1 mag) between the observed and predicted location of the red peak. As pointed out above this may be due to, and is consistent with, the departure of the color term from the linear correction adopted for objects with $(B-V) > 1.2$. Note that the agreement is much better in $(V-I)$ for which the contribution from color terms are expected to be negligible.

Traditionally, the observed splitting in the color peaks has been used to determine the local normalization of halo stars in the solar neighborhood. Note in this context the difference in the amplitude of the counts in the blue peak in the magnitude range $20 < V < 21$, which is seen in both $(B-V)$ and $(V-I)$. Most photometric surveys at faint magnitudes (e.g., Reid & Majewski 1993) have relied on pencil-beam surveys covering a small fraction of a degree. Therefore, the number of observed objects per bin has been very small, leading to large uncertainties in the derived model parameters. The EIS sample, covering ~ 1.3 square degrees, represents a significant improvement and may allow for a better determination of these parameters.

Finally, it is interesting to point out the existence of a population of blue objects, in particular, the suggestion of a peak at $(B-V) \sim 0.15$ observed at faint magnitudes ($20 < V < 21$). This peak does not match the location and the amplitude of the peak predicted by the white dwarf population assumed in

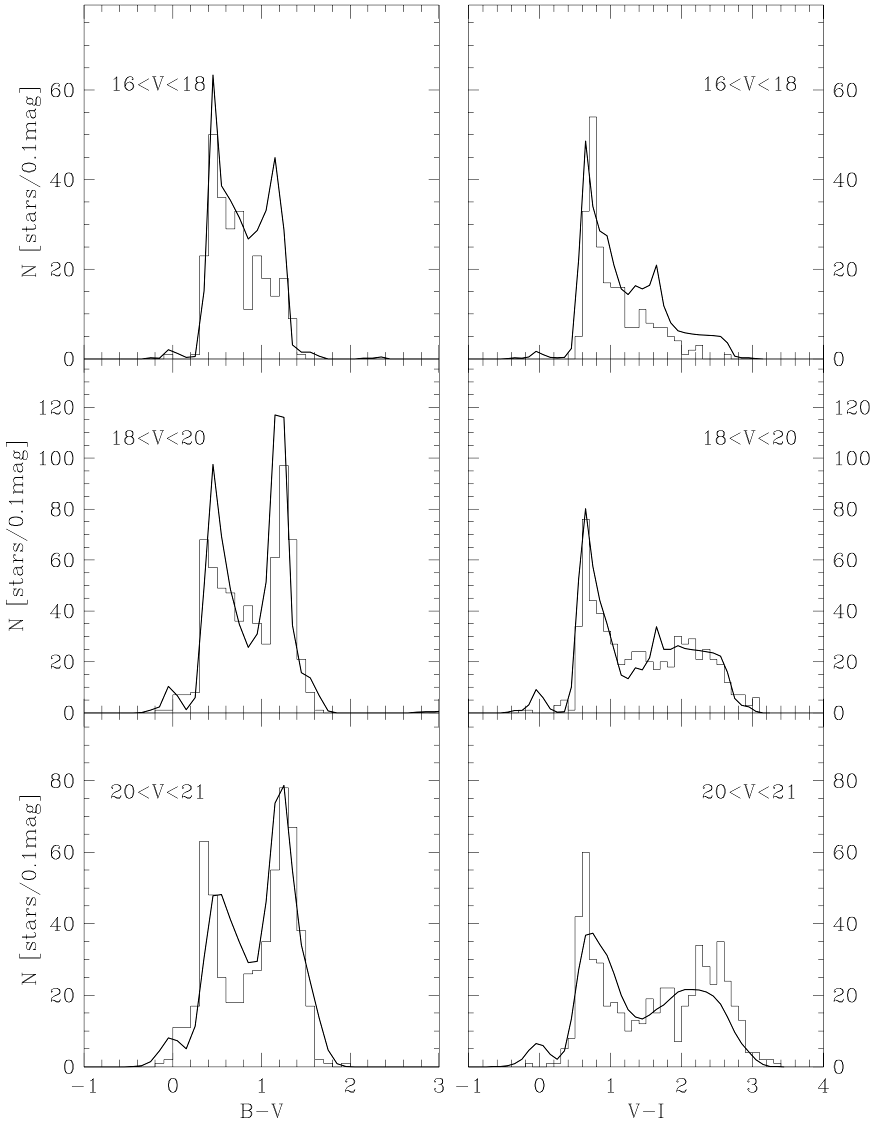

Fig. 14. Color distribution for point-sources for different magnitude intervals as indicated in each panel. Also shown are predictions for the galactic model of Méndez & van Altena (1996).

the model. Instead the observed blue objects could consist of a mix of white dwarfs, blue horizontal branch stars or perhaps halo field blue stragglers. Further investigation on the nature of these objects seems worthwhile.

The results demonstrate that the stellar color catalog being produced is by and large consistent with model predictions and the observed differences may possibly point to deficiencies in the model which should be further investigated by interested groups. Although primarily driven by other goals, the above discussion shows that the EIS data is also useful for galatic studies.

3.2. Galaxies

In order to evaluate the quality and the depth of the galaxy samples, galaxy counts in the different passbands are shown in Fig. 15 and compared to those determined for patch A and by other authors as indicated in the figure caption. In these comparisons the I magnitudes of Lidman & Peterson (1996) have been shifted by +0.04 mag and those measured by Postman et al. (1996) by -0.43 mag to bring them into the Johnson-Cousins system. A small correction (-0.02 mag) has also been applied to the V counts of Postman et al. . No corrections were made to the Arnouts et al. (1997) data. As can be seen there is a remarkable agreement between the EIS counts and those obtained by other authors. They are also consistent with the counts determined from patch A, down to $V \sim 24$ and $I \sim 22.5$. As emphasized in Paper I even for single exposures EIS reaches fainter magnitudes than previous data used for cluster searches.

The overall uniformity of the EIS galaxy catalogs can be examined using the two-point angular correlation function, $w(\theta)$. Indeed, $w(\theta)$ is a very efficient tool for detecting any kind of artificial patterns (such as a grid with scale comparable to an EMMI frame) or possible gradients in the density over the field (which could result from large-scale gradients of the photometric zero-point). Departures from uniformity should affect the correlation function especially at faint magnitudes.

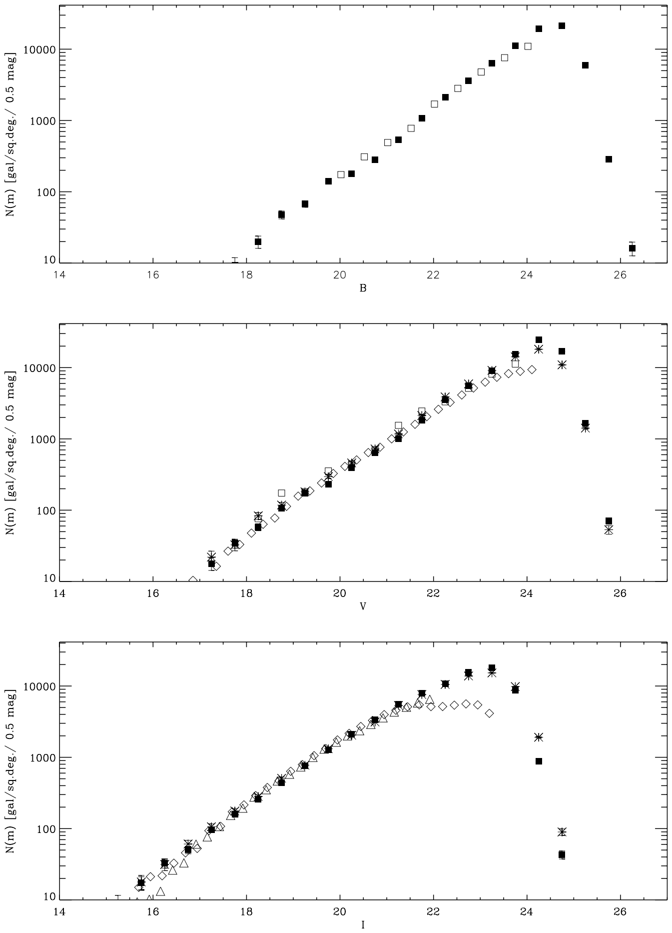

Fig. 15. EIS patch B galaxy counts (filled squares) in different passbands (B, V, I, from top to bottom) compared to the counts obtained by: Lidman & Peterson (1996, triangles), Postman et al. (1996, diamonds) and Arnouts et al. (1997) (open squares), as provided by the authors. Also shown are the counts obtained in patch A (stars) for the V and I-band. The counts from other authors have been converted to the Johnson-Cousins system, as described in the text.

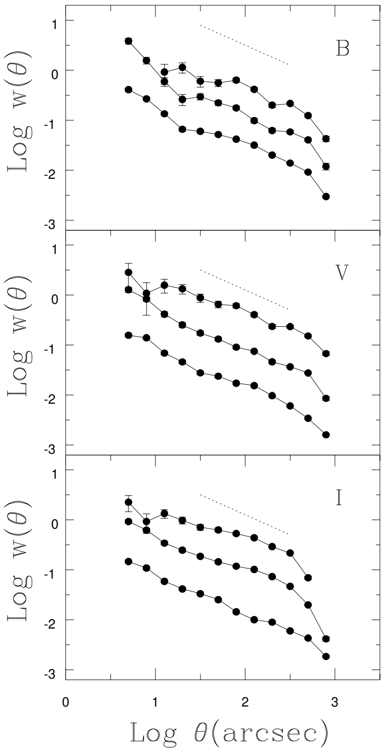

Fig. 16. The angular two-point correlation function calculated for patch B, in the B, V, and I bands as indicated. In each panel the three curves correspond (from top to bottom) to the limiting magnitudes 21, 22, 24 (in B); 20, 22, 24 (in V); 19, 21, 23 (in I). The dotted line represents a power law with a slope of -0.8. The error bars are 1σ errors obtained from 10 bootstrap realizations.

Fig. 16 shows $w(\theta)$ obtained for each of the three passbands B, V, and I, using the estimator proposed by Landy & Szalay (1993). The calculation has been done over the area defined above (see Fig. 7). The error bars are 1σ errors calculated from ten bootstrap realizations. The angular correlation function is, in general, well described by a power law $\theta^{-\gamma}$ for angular scales extending out to $\theta \sim 0.5$ degrees, with a value of γ in the range 0.7–0.8. The absence of any strong feature at the scale of the individual survey frame should be noted. Furthermore, no significant variations of the slope are detected, except at the bright end in all the three passbands. In this case $w(\theta)$ is somewhat flatter than at fainter magnitudes. A possible explanation is the presence of the nearby cluster (ACO S84) at $z \sim 0.1$ located near the center of the patch. To test this hypothesis the correlation function was recomputed by discarding a square region of about 0.2 degrees on the side centered at the nominal position of the cluster. Using the pruned sample yields a steeper correlation function for the patch, consistent with the expected slope of 0.8. These results show the uniformity of the EIS catalogs, once obviously bad frames, selected on the basis of seeing and limiting isophote, are discarded.

The angular correlation function can also be used to verify the consistency of the photometric zero-points determined for patches A and B. This can be done by studying the amplitude of the angular correlation function as a function of limiting magnitude and comparing the results obtained for the two patches. Fig. 17 shows the amplitude of the angular correlation function at a scale of 1 arcmin, A_w, as a function of the limiting magnitude in the different passbands. This amplitude is calculated from the best linear-fits over the range $\sim$ 10–200 arcsec of $w(\theta)$ shown in Fig. 16. For V and I one finds good agreement between the results for the two patches especially at the faint end. The differences seen in the bright end are fully accounted for by the presence of the nearby cluster described above. The plot shows the amplitude of the correlation with and without the cluster. As can be seen once the cluster is removed, the amplitude at the bright end decreases and shows a good agreement with the estimate from patch A. Similarly, one finds good agreement with the results obtained by other authors such as: in the B band, Roche et al. (1993) ($23 \le B \le 24$) and Jones et al. (1987) ($19 \le B \le 21$); in the V band, Woods & Fahlman (1997) (V=24); and in the I band, Postman et al. (1998) ($19 \le I \le 23$). The amplitude of the angular correlation function as determined

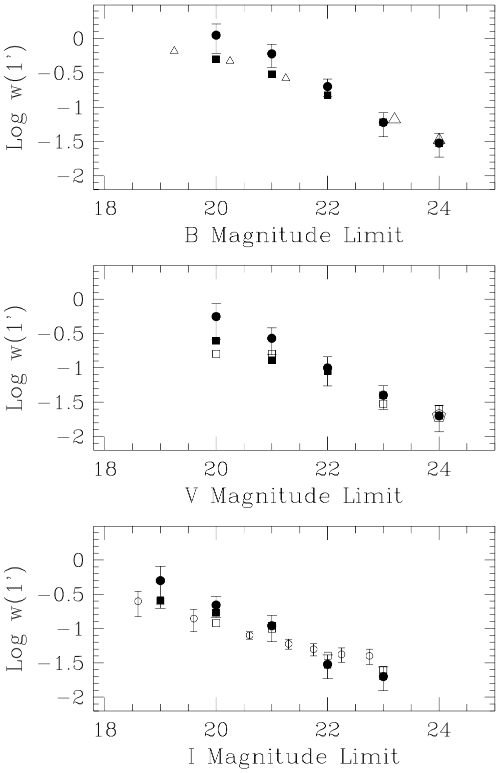

Fig. 17. Amplitude of the correlation function measured at 1 arcmin for patch A (open squares), and patch B (full circles) and after removing the nearby S84 cluster (full squares). These results are compared to those from Roche et al. (1993) (big open triangles) and Jones et al. (1987) (small open triangles) in the B band, from Woods & Fahlman (1997) in the V band (open pentagon), and from Postman et al. (1998) in the I band (open circles).

from the EIS galaxy catalogs are consistent with those obtained by various authors over the entire range of magnitude. Note that for $I \gtrsim 22$ the EIS points lie slightly below those recently computed by Postman et al. (1998).

In summary, the above results are further evidence that the EIS galaxy catalogs are uniform within a patch, that the zero-points for the different patches are consistent and are in good agreement with external data.

4. Summary

In this paper multicolor data for patch B covering about 1.7 square degrees near the SGP have been presented. The quality of single band and color catalogs have been assessed by comparisons of basic statistics such as number counts, color distribution, and angular correlation function, with model predictions and results from other authors. The results indicate that the EIS object catalogs are suitable for the science goals of the survey leading to consistent results when compared to other data. Furthermore, one finds good agreement between the results derived from the catalogs extracted from patches A and B.

The work being carried out is essential in the preparation of the final release of the EIS data. While the production of single-frame catalogs is straightforward, the preparation of a catalog covering the whole patch requires some experimentation in order to fine-tune the parameters and verify its uniformity, completeness, and reliability. Multicolor data adds to the complexity of the task of catalog production and further work in the preparation of well understood color catalogs is required. The experience gained so far points out the need for a sustained effort in the development of techniques and tools which will allow for: 1) the production of more customized catalogs for different science goals, essential for public surveys; 2) the exploration of the multi-dimensional space offered by multicolor data; 3) the cross-correlation of the detected objects with the increasing number of databases available in different wavelengths. Searches in this multi-dimensional space offer unique science opportunities and the implementation of suitable tools for its exploration represent a major challenge for the efficient use of imaging surveys carried out with the specific purpose of producing targets to feed 8-m class telescopes.

The full range of products for patch A and B in the form of astrometric and photometric calibrated pixel maps, object catalogs, candidate target lists (Zaggia et al., 1999) and on-line co-added section images can be found at "http://www.eso.org/eis". New products will be added incrementally as they become avaialble. Further information on the project are available on the World Wide Web at "http://www.eso.org/eis".

Acknowledgements. We thank all the people directly or indirectly involved in the ESO Imaging Survey effort. In particular, all the members of the EIS Working Group for the innumerable suggestions and constructive criticisms, the ESO Archive Group and ST-ECF for their support. We also thank C. Lidman for providing his images, zero-points and catalogs. We are also grateful to the DENIS consortium for making available some of their survey data. The DENIS project development was made possible thanks to the contributions of a number of researchers, engineers and technicians in various institutes. The DENIS project is supported by the SCIENCE and Human Capital and Mobility plans of the European Commission under the grants CT920791 and CT940627, by the French Institut National des Sciences de l'Univers, the Education Ministry and the Centre National de la Recherche Scientifique, in Germany by the State of Baden-Wurttemberg, in Spain by the DGICYT, in Italy by the Consiglio Nazionale delle Richerche, by the Austrian Fonds zur Förderung der wissenschaftlichen Forschung und Bundesministerium für Wissenschaft und Forschung, in Brazil by the Fundation for the development of Scientific Research of the State of São Paulo (FAPESP), and by the Hungarian OTKA grants F-4239 and F-013990 and the ESO C & EE grant A-04–046. Our special thanks to A. Renzini, VLT Programme Scientist, for his scientific input, support and dedication in making this project a success. Finally, we would like to thank ESO's Director General Riccardo Giacconi for making this effort possible.

References

Arnouts S., de Lapparent V., Mathez G., et al., 1997, A&AS 124, 1
Bahcall J.N., 1986, ARA&A 24, 577
Deul E., Bertin E., da Costa L., et al., 1999, EIS Explanatory Supplement, in preparation
Deul E., 1999, private communication

Jones L.R., Shanks T., Fong R., 1987, In: Bergeron J., Kunth D., Rocca-Volmerange B., Tran Thanh Van J. (eds.) High Redshift and Primeval Galaxies. Editions Frontière, Gif-sur-Yvette, p. 29
Landolt A.U., 1992a, AJ 104, 340
Landolt A.U., 1992b, AJ 104, 372
Landy S.D., Szalay A., 1993, ApJ 494, 1
Lidman C., Peterson B., 1996, MNRAS 279, 1357
Méndez R.A., and van Altena W.F., 1996, AJ 112, 655
Nonino M., Bertin E., da Costa L.N., et al., 1999, A&AS, in press (paper I)
Olsen L.F., Scodeggio M., da Costa L.N., et al., 1999, A&A, astro-ph/9807156 (paper V)
Postman M., Lubin L.M., Gunn J.E., et al., 1996, AJ 111, 615
Postman M., Lauer T.R., Szapudi I., Oegerle W., 1998, ApJ, in press
Reid N., Majewski S.R., 1993, ApJ 409, 635
Renzini A., da Costa L.N., 1997, The ESO Messenger, No 87, p. 23
Roche N., Shanks T., Metcalfe N., Fong R., 1993, MNRAS 263, 360
Woods D., Fahlman G., 1997, ApJ 490, 11
Zaggia S.R., Hook I., Mendez R.H., et al., 1999, A&AS, astro-ph/9807152 (paper IV)